Energy 171 (2019) 853–865

Contents lists available at ScienceDirect

Energy

journal homepage: www.elsevier.com/locate/energy

Characterization of woodstove briquettes from torrefied biomass and coal

Anna Trubetskaya [a, b, *], James J. Leahy [c], Elena Yazhenskikh [d], Michael Müller [d], Peter Layden [e], Robert Johnson [e], Kenny Ståhl [f], Rory F.D. Monaghan [a, b]

[a] School of Engineering and Ryan Institute, National University of Ireland Galway, Galway, Ireland
[b] Research Centre for Marine and Renewable Energy, Galway, Ireland
[c] Department of Chemical Sciences, University of Limerick, Limerick, Ireland
[d] Forschungszentrum Jülich GmbH, 52425, Jülich, Germany
[e] Arigna Fuels, Arigna Carrick-on-Shannon Co. Roscommon, Ireland
[f] Department of Chemistry, Technical University of Denmark, Kemitorvet B206, 2800, Kongens Lyngby, Denmark

ARTICLE INFO

Article history:
Received 11 October 2018
Received in revised form
15 December 2018
Accepted 13 January 2019
Available online 18 January 2019

Keywords:
Olive stones and coal briquettes
Torrefaction
Binders
Char
XμCT
Solid-state NMR

ABSTRACT

Using waste biomass materials offers the potential to reduce the greenhouse gas emissions from fossil fuels. Torrefaction is very useful for improving the fuel properties of biomass in order to better match those of coal. The aim of this work is to compare the properties of torrefied low quality biomass briquettes against coal equivalents. The composition of the briquettes was characterized by ^{13}C CP/MAS, proximate analysis, and X-ray diffraction and the results were compared with equilibrium calculations. In addition to these techniques, we report for the first time on the use of XμCT for characterizing such materials. The XμCT analysis showed that the briquette structure contains carbon, binder and inorganic matter, with quartz retained from the original feedstock in torrefied biomass and coal briquettes. The CO_2 reactivity of pulverized briquettes was investigated by thermogravimetric analysis. Results showed that the inorganic matter influences the reactivity less than the organic composition and porosity. Importantly from a technological standpoint, the increase in binder concentration and replacement of starch with resin binder did not influence the reactivity and calorific value of a pulverized briquette.

1. Introduction

The use of renewable energy from biomass is one of the few proven, cost-effective and available technologies that can decrease CO_2 emissions. Ireland is one of the least forested countries in Europe with less than 10.5% of forest (≈697,600 ha) [1]. The vast and growing amount of agricultural and food waste has become a major concern throughout the world; within the EU, approximately 700 million tons of agricultural wastes are generated annually [2]. The Mediterranean area has significant bioenergy potential from agricultural residues, especially from olive oil as they are responsible for over 98% of worldwide production [3]. Olive stones represent on average 13.6% of the fruit mass with the low lipid content (4 wt. %) and thus, are used in olive mills to produce low quality oils [4]. The remaining olive stones from olive mills can be dried and further used as an energy resource. Direct combustion of olive stones may encounter technical and economic drawbacks associated with the low energy density, high moisture content and limited fixed carbon fraction [5]. Conversion of olive residues to high-density briquettes using torrefaction as a pretreatment process is a potential solution to solid waste problems as well as to the lack of locally available fuel wood in Ireland.

The lower carbon, sulfur and chlorine contents of biomass have a great potential to reduce emissions formed during combustion [6]. Specifically, emissions such as SO_2, CO_2, polycyclic aromatic hydrocarbons (PAH) and chlorinated micro pollutants (e.g. dioxins) are reduced [7]. These environmental benefits are additional to those associated with the renewable nature of biomass, making it a climate-friendly briquette component. Torrefaction of biomass has been found to reduce particulate emissions from combustion by ≈ 40% when compared to the raw feedstock [8]. Torrefaction is a mild pyrolysis process that converts biomass into a higher carbon material with increased energy density and decreased oxygen

* Corresponding author. School of Engineering and Ryan Institute, National University of Ireland Galway, Galway, Ireland.
E-mail address: anna.trubetskaya@nuigalway.ie (A. Trubetskaya).

https://doi.org/10.1016/j.energy.2019.01.064
0360-5442/

content. The torrefaction process removes many of the smoke producing volatile components from biomass whilst leaving sufficient residual volatile matter content for enhanced fuel combustion. Torrefied biomass particles are loose and nonuniform due to decreased hemicellulose content [9]. One way to improve the torrefied biomass handling and combustion properties is by densification into briquettes. Briquettes made from torrefied biomass have many advantages over torrefied feedstock which include reduction of dust, improved handling properties and higher bulk density (up to 66% greater). This decreases the cost of shipment and storage [10]. Properties of the original feedstock such as density, moisture content, heating value, ash content, impact and compressive strength affect the quality of torrefied material. Temperature and residence time are the key parameters which have an influence on the degree of torrefaction [11]. In general, briquettes made from raw eucalypt particles showed on average greater moisture content than briquettes made from torrefied feedstocks [12]. Torrefaction temperatures from 250 to 270°C are used in the industrial process to make briquettes more hydrophobic and more stable against chemical oxidation and microbial degradation [13,14]. In addition, low torrefaction temperatures from 250 to 300°C are used to prevent excessive mass losses from volatile components and alkali metal release that may increase the reactivity of torrefied biomass [15]. Treatment at higher torrefaction temperatures decreases the oxidation reactivity of biomass char due the increase in torrefaction severity [16]. In order to achieve a better densification, the type of bonding and mechanical interlocking are the key factors to understand. The ash content of wood and herbaceous biomass remains largely unchanged during torrefaction [17,18]. Operating parameters (280°C, 30 min) have been suggested as the optimum conditions for the torrefaction of olive stones [19]. Torrefied biomass particles are more difficult to densify compared to raw biomass particles which results in the poor storage and transport characteristics of torrefied biomass pellets [20,21]. Hardness and durability of torrefied biomass briquettes can be improved by the addition of binders [10]. A wide range of combustible binders (e.g., natural or synthetic resins, lignin, starch, etc.) and non-combustible additives (e.g., inorganic clay minerals, cement, etc.) can be used [22–24]. Guar gum and starch are selected as the most suitable binders for briquettes from pulverized coal [25]. The calorific values and fixed carbon content of briquettes decreased with the increased binder concentration, decreasing the burnout time in a woodstove [26]. Binder concentration, biomass particle size, cure temperature and time have the greatest influence on briquette quality [27,28]. The effect of binder concentration and type on the structure and reactivity of torrefied olive stones and coal briquettes has been rarely studied.

Torrefaction combined with briquetting is a promising way for olive mill waste pretreatment and bioenergy feedstock production [3]. Binders used in briquetting are generally much more expensive than the torrefied fuel itself, and thus a balance has to be found between cost and quantity of binder agents [29,30]. Knowledge about the influence of binder type and concentration on the briquette structure and reactivity is important to improve the quality of a torrefied olive stone briquette for easy handling/transportation and smokeless combustion or gasification in household stoves. In comparison with the traditional woodstoves, gasification stoves utilize combustion smoke that gives control over oxidation rate leading to the efficient consumption of briquettes [31]. Therefore, CO_2 gasification reactivity becomes a key variable that must be understood in potential replacements for traditional woodstoves. Despite torrefaction of diverse resources being reported in the literature [3,17,32], there is a gap of information in the implementation of this technique as an efficient management treatment to minimize organic waste. The specific objectives of this study were to: (1) develop structure-property relationships governing the CO_2 reactivity of briquettes from torrefied biomass and pulverized coal, and (2) determine the composition of feedstock and binder that is suitable for application in torrefaction process. To achieve these objectives this project utilizes novel characterization techniques which bring a greater technical understanding to the roles of the individual components of the feedstocks in determining reactivity.

2. Materials and methods

Woodchips and olive stones were chosen for the torrefaction study. Sitka Spruce (Picea sitchensis) from various sites in County Leitrim (Ireland) was harvested in 2017. The age of the Sitka Spruce was 25 years. The logs were chipped to pass a 50 mm screen after air drying to <45% moisture content. Washed olive pits (Olea europaea) were sourced from Spain and are a by-product of the olive oil industry where they are separated, crushed to < 3 mm and air dried. The low ash-containing woodchips and olive stones have a similar ash content which is high in K, Ca and Si elements. Both feedstocks also contain a similar guaiacyl-syringyl (GS) lignin type, with olive stones also having a wide variety of phenolic compounds. Woodchips and olive stones were selected to investigate the effect of differences in organic matter (cellulose, hemicellulose, lignin, extractives) on the torrefied biomass structure and reactivity. The properties of torrefied briquettes were compared with briquettes from anthracite coal that was supplied from South Wales, UK.

Woodchips and olive stones were torrefied under similar operating conditions at the Arigna Fuels plant. A total of 50 t of biomass was continuously torrefied during a 24 h long experiment. A sample of the torrefied material was collected at the end of the experiment and held at ambient temperature in a desiccator. The properties of raw and torrefied biomass were compared with those of anthracite and coal briquettes with regard to CO_2 reactivity, surface structure, chemical composition, particle size and shape using a thermogravimetric analyzer, X-ray microtomography, scanning electron microscopy, NMR analysis, sieving, 2D dynamic imaging, laser diffraction, and X-ray diffraction in combination with the thermodynamic calculations. Based on previous work [33], the reactivity of torrefied material and milled coal briquettes was analyzed by exposing samples in 20% volume fraction CO_2 to avoid mass transfer limitations. The effect of a binder concentration and binder type on the properties of briquettes was investigated by increasing the starch concentration in torrefied woodchip briquette and using resin or starch binders in a coal briquette. The porosity and pore size of original material, torrefied biomass, anthracite, and coal briquettes were determined using a helium pycnometer and a mercury intrusion porosimeter.

2.1. Biomass torrefaction and briquetting

Fig. 1 illustrates the biomass torrefaction and briquetting processes at Arigna Fuels. The torrefaction of woodchips was carried out at 280°C, whereas olive stones were torrefied at a higher treatment temperature. The dryer and pyrolysis reactors are both heated indirectly with thermal oil. Liquefied petroleum gas (LPG) is used to heat the plant initially and start the torrefaction process, but when gases are produced, these are combusted in a thermal oxidizer to provide heat to the drying and torrefaction processes and no further heat source is required. The heat recovered from thermal oil is used for the drying of coal briquettes produced at the integrated coal briquetting pilot plant. The torrefied biomass is cooled to room temperature, further crushed and briquetted.

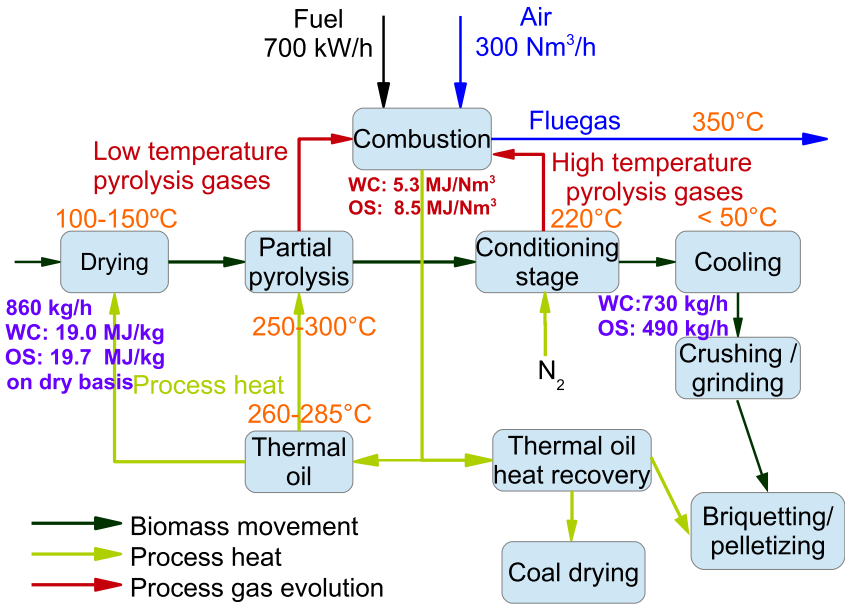

Fig. 1. Arigna torrefaction plant schematic.

2.2. Biomass and char characterization

Feedstock pre-treatment. The torrefied biomass and anthracite-based briquettes were comminuted in a laboratory-scale pulverizing mill LM1-P (LABTECHNICS, Australia) and sieved to a particle size of <0.3 mm.

Thermogravimetric analysis. Char samples were crushed to a fine powder in a mortar with a ceramic pestle. Char reactivity was analyzed by exposing samples to a reactive gas consisting of 20% volume fraction CO_2 in a thermogravimetric instrument TGA/DSC 1 STARe System (Mettler Toledo, USA). For each experiment, 7 mg of sample was loaded into an Al_2O_3 crucible and heated from 30 to 1100°C in CO_2 at a constant heating rate of 10°C min^{-1}. The kinetic parameters of the char samples were derived by the integral method presented by Coats and Redfern [34]. Through integral transformation and mathematical approximation, the linear equation was expressed in the form:

$$ln\left(-\frac{ln(1-X)}{T^2}\right) = ln\left(\frac{A\cdot R}{\kappa\cdot E_a}\right) - \frac{E_a}{R\cdot T} \quad (1)$$

In equation (1), κ is the heating rate, R is the gas constant and X is the conversion. A plot of ln (-ln (1-X) T^{-2}) versus T^{-1} gives a straight line whose slope and intercept determine the values of the activation energy (E_a) and pre-exponential factor (A). Reactivities of the char samples were compared using reaction rates calculated from the derived kinetic parameters (A and E_a) at a fixed gasification temperature of 1000°C.

X-ray microtomography. The full 3D microstructure of the olive stone or coal briquettes was scanned using x-ray microtomography (XMT, μCT, XRM) [35–37], and characterized quantitatively using 3D image analysis. A briquette was sliced in a 5x5x5 mm^3 cube that was scanned using the XMT instrument Zeiss Xradia 500 Versa (Carl Zeiss X-ray Microscopy, Pleasanton, CA, USA). No compression was used in order to prevent any artificial modification of the wood particles [38]. The field of view was 4.03 × 4.03 mm^2 and the spatial resolution in terms of voxel size was 3.98 μm. The x-ray tube voltage and tube power was 50 kV and 4 W, respectively. 3201 projections (radiographs) were collected, with exposure time 1 s, over a sample rotation of 360°, resulting in a total scan time of 2.5 h. The reconstructed briquette cube structure corresponds to a rectangular region of diameter 3.98 mm (top), 3.95 mm (bottom) and height 4.03 mm. Images were cropped to obtain a 2.5 mm cubed section. The segmentation was carried out by thresholding, using Otsu's method [39]. The images were segmented into 3 phases based on greyscale values of inorganic matter, feedstock, and binder. Porosity was calculated using 3D volume of each phase [36,37]. The 3D quantitative image analysis and visualizations were carried out using TXM3D viewer software (Xradia Inc., Concord, USA) and Avizo 8.1 software (FEI, Germany).

X-ray diffraction. The crystalline constituents of biomass, anthracite and torrefied samples were characterized using a Huber G670 X-ray diffractometer with a copper tube, a quartz monochromator (CuKα1 radiation, λ = 1.54,056 Å), using an imaging strip covering 100° as a detector for 4 h. The diffractometer was operated in transmission mode with the sample placed on tape in a thin layer and placed on a rotating disc-holder. The phase analyses were done in the Crystallographica Search-Match software (Version 3,1,0,0) and the ICDD PDF4 database. The multiple phase fitting of the PXRD patterns and crystallite size analysis were carried out with the WINPOW Rietveld software. The refined backgrounds have been subtracted in the displayed PXRD patterns.

Thermodynamic calculations with FactSage. Thermodynamic calculations were performed using the computational package FactSage [40]. The commercial database FToxid combined with the dataset FactPS for pure substances along with the new GTOX oxide database (Research Center Jülich and GTT-Technologies, Germany) [41] and the commercial database for pure substances (SGPS) were used for the equilibrium calculations under defined conditions (chemical composition of a system, temperature, pressure). All available phase relations were taken into account by calculation: the Gibbs energy of a system is minimized in order to find the equilibrium state. The results were obtained for equilibrium conditions only, the possible kinetic effects are not considered.

SEM microscopy. SEM/EDS analysis of char was conducted on a high-resolution field emission microscope SU-70 (Hitachi, Japan) under high vacuum in order to understand char structural properties. Prior to analysis, char samples were coated with a thin layer of gold (2 min, 20 mA) using an Edwards S150B Sputter Coater to avoid sample charging.

Mercury intrusion porosimetry. Pore size distribution and porosity of char samples were determined by a Pascal mercury intrusion porosimeter system equipped with two instruments. Porosity in the ultramacro and macropore regions was measured by Pascal 140 porosimeter (Micromeritics, Germany) at the low pressures (up to 400 kPa). The Pascal 440 porosimeter equipped with a dilatometer (Micromeritics, Germany) was used to determine the pore size from 1.8 to 7500 nm at high pressures up to 400 MPa. To access the pores and voids within feedstock particles, samples were degassed at room temperature prior to the measurement. Prior to the porosity analysis, raw feedstock, torrefied biomass and coal briquettes were dried at 50°C in an oven desiccator for 48 h.

Pore volume and size. The pore sizes in the char were distinguished into three categories: micropores (1.8–80 nm), mesopores (80–500 nm) and macropores (0.5–58 μm) [42,43]. The pore volume can be derived from the quantity of intruded mercury. The pore size distribution is determined according to the Washburn equation [44]:

$$D_p = -\frac{4\gamma cos\Theta}{p} \quad (2)$$

In equation (2), p is the pressure and Θ is the angle of contact that is assumed to be equal to 141° [45]. γ is the surface tension that is equal to 0.48 N m^{-1} [42]. The median pore diameter (D_{md}) is defined as the pore diameter at which 50% of total intrusion was reached. The average pore diameter (D_{pa}) is calculated, assuming that all pores are cylindrical, in equation (3) [46]:

$$D_{pa} = -\frac{4V_{cum}}{SSA} \quad (3)$$

The cumulative pore volume distribution is calculated in equation (4) [46]:

$$V_{cum}(D) = \frac{-dV_p}{dlogD_p} \quad (4)$$

Helium pycnometry. Skeletal density is defined in accordance with DIN 66,137 (Part 2) standard by equation (5) [47]:

$$\rho_s = \frac{m_s}{V_s} \quad (5)$$

In equation (5), m_s and V_s are the mass and volume of solid particles. The calculation of skeletal density excludes the porosity within the particles and the interparticle voids. Skeletal density was determined using a helium pycnometer (POTOTEC GmbH, Germany) at room temperature.

2D dynamic imaging analysis. Particle size and shape were measured using a CAMSIZER (Retsch Technology, Germany), designed for particles ranging from 0.03 to 30 mm in size. Particle shadows were captured by two cameras; a zoom camera, designed for the analysis of smaller particles, and a basic-camera that was able to detect larger particles. The projected area of the particle was determined using CAMSIZER 6.3.10 software (Retsch Technology, Germany). Particle size distribution, based on volume, is represented by the $x_{Ma,min}$ diameter. For the particle size analysis, ca. 100 mg of a dry sample was used. Particle size was characterized by sphericity (SPHT) and aspect ratio (AR). The results are presented as a cumulative particle size distribution, based on volume (q_3).

Solid-state NMR Spectroscopy. Solid-state NMR data were acquired on a Bruker Avance III HD wide-bore NMR spectrometer operating at $B_0 = 9.4$ T. This magnetic field strength corresponds to ^{1}H and ^{13}C Larmor frequencies of $\nu_0(^1H) = 400.14$ and $\nu_0(^{13}C) = 100.62$ MHz, respectively. Samples were packed under ambient conditions in 4 mm o. d. zirconia rotors with Kel-F caps, and data were acquired under MAS conditions on a triple resonance (X/Y/^{1}H) 4 mm Bruker MAS probe operating in double resonance mode. The MAS frequency for all samples was 12 kHz. Chemical shift values in ^{13}C NMR spectra were referenced to TMS at $\delta = 0$ ppm by changing the field such that the methylene peak in the ^{13}C NMR spectrum of adamantane resonated at 38.48 ppm [48]. Carbon-13 NMR spectra were collected using a cross polarization with total suppression of spinning sidebands (CP/TOSS) pulse sequence which employs 5 π pulses and a 243 step phase cycle for sideband suppression [49,50]. Carbon-13 180° pulses in this sequence were 8 μs in length. Proton decoupling at a frequency of 83 kHz was applied during FID acquisition using the SPINAL64 decoupling sequence [51]. Proton T_1 relaxation times were determined using the saturation recovery pulse sequence, and recycle delays in cross polarization NMR experiments were set to greater than $5 \cdot T_1$. Note the recycle delays were much longer than the optimal $1.3 \cdot T_1$ due to restrictions from the duty cycle. Proton 90° pulses were 3 μs in length and the pulse power level was optimized using a sample of powdered adamantane. Contact times used for cross polarization were optimized for each sample and ranged from 0.1 to 2 ms. The number of transients collected for each ^{13}C NMR spectrum ranged from 2430 to 4860. Line broadening was applied prior to Fourier transformation. A detailed overview of NMR acquisition and processing parameters is shown in the supplemental material (Table S-3). Data were acquired and processed using TopSpin 3.5 pl 7 software.

3. Results

Ultimate and proximate analysis of olive stones, woodchips, and anthracite is shown in Table 1.

The ash content of torrefied material was greater than that of raw woodchips and olive stones. However, ash elemental composition of raw biomass and torrefied material was similar, indicating that low temperature treatment has no influence on the biomass ash composition. The ash content of pulverized coal briquettes using starch or resin was lower than that of anthracite. In addition, the content of alumina and silica slightly decreased during coal briquetting. Analysis of biomass constituents (cellulose, hemicellulose, acid-soluble lignin, acid-insoluble lignin, and extractives) was conducted according to NREL technical reports [52–54] and Thammasouk et al. [55], and shown in Table 2.

3.1. Reactivity

Fig. 2 shows differential weight loss curves (DTG) for CO_2 gasification (20% by volume) of raw woodchips and olive stones, torrefied material, torrefied woodchips with the high starch content, anthracite, pulverized coal briquette using starch or resin as a binder. The DTG curve of raw woodchips shows a double peak at 340 and 520°C, whereas the DTG curve of olive stones shows a triple broad peak at 275, 340, and 500°C. The decomposition of holocelluloses occurs in the temperature range from 275 to 310°C, whereas the decomposition rate of lignin increases over a broader range from 220 to 700°C [56]. Decomposition in the temperature range from 500 to 520°C is attributed to CO_2 gasification of the char after the release of volatile matter at lower temperatures [57].

Torrefied woodchips showed a double broad peak due to the torrefaction at 280°C, whereas olive stones showed a single broad peak due to the torrefaction at about 20°C greater temperature. This indicates an influence of heat treatment temperature on the CO_2 gasification, confirming the previous results of Xue et al. [58]. Torrefied woodchips and torrefied olive stones show either a single or a double broad peak, both of which indicate a heterogeneous feedstock mixture with respect to reactivity [59,60]. Maximal

Table 1
Proximate, ultimate and ash compositional analysis.

	Wood-chips	Olive stones	Anth-racite	Torrefied wood-chips	Torrefied woodchips (high starch)	Torrefied olive stones	Coal bri-quette (starch)	Coal bri-quette (resin)
Proximate analysis								
Moisture, (wt. % ar)	14.9	15.5	2.7	2	4.9	0.6	0.9	2.9
Ash at 550°C/815°C, (wt. % db)	0.5	0.8	9.9	1	1.5	2.1	4.8	4.5
Volatiles, (wt. % db)	78.9	76	15.8	67.7	54.5	22.2	15	14.1
HHV, (MJ kg^{-1} ar)	18.7	20.3	32.2	22.3	22.9	22.7	33.2	32.4
LHV, (MJ kg^{-1} ar)	17.2	18.8	31.5	21.3	21.8	21.7	32.9	31.9
Ultimate analysis, (wt. %, dry basis)								
C	46.7	44.8	72.3	55.5	56.8	54.9	82.5	86.6
H	5.7	5.8	2.9	5	5	5	2.8	2.4
N	0.2	0.2	1	0.03	1	1	1.7	1.6
O	46.4	48.3	13.2	38.5	35.7	36.9	6.5	3
S	0.03	0.1	0.7	0.02	0.02	0.1	1.7	1.9
Cl	0.01	0.01	0.03	0.01	0.01	0.01	0.01	0.01
Ash compositional analysis, (mg kg^{-1}, dry basis)								
Al	50	100	12,000	100	150	250	9500	9100
Ca	1300	1650	3500	1700	1600	1500	3400	3200
Fe	50	70	7200	130	200	250	7000	6800
K	900	1600	2000	1560	1800	1900	2000	2300
Mg	200	150	350	130	100	200	450	450
Na	100	300	2000	300	450	650	2250	2100
P	200	100	800	100	100	150	850	750
Si	500	1800	41,000	2500	2500	2000	38,000	37,000
Ti	4	10	700	10	20	20	650	600

Table 2
Lignocellulosic composition of woodchips and olive stones.

Biomass	Cellulose	Hemi-cellulose	Lignin		Extractives
			acid insoluble	acid soluble	
Olive stones	25.4	25.6	28.9	1.6	4.6
Woodchips	42.6	17.6	26.8	0.5	3.8

reaction rates of torrefied woodchips and olive stones were about 20 and 40°C greater than that of raw biomass. The reactivities of torrefied woodchips and material with greater starch content were nearly identical, indicating less influence of starch concentration on the reactivity of pulverized biomass briquettes. Similar tendencies were observed for the anthracite and pulverized coal briquette using starch or resin as a binder. The DTG peak of pulverized coal briquettes using resin as a binder was slightly broader than the DTG peaks of anthracite and pulverized coal briquette using starch as a binder. This shows that the use of resin as a binder decreases the reactivity of coal briquette and thus, increases the burnout time in a woodstove.

3.2. X-ray microtomography

Fig. 3 shows the 3D cross-sectional slices obtained from XμCT measurements for olive stone briquettes using the starch binder and coal briquettes using either a starch or resin binder. The characteristic features of briquettes such as coal or biomass particles, binders and inorganic matter are observed for all scanned samples.

The spatial resolution of 3.98 μm is sufficient for observing most features of the feedstock particles and binders, providing physically reasonable structural assessments. The bright volumetric areas in Fig. 3 were related to the presence of inorganic matter. The XμCT images indicated that coal particles in briquettes were less elongated and less porous than biomass particles, as shown in the supplemental material (Fig. S-16). The greater level of voids, filled with a binder in biomass briquettes than in both coal briquettes reflects the greater porosity of torrefied olive stones. The porosity calculated from XμCT scans corresponds to material characteristics measured by mercury intrusion porosimetry. Table 3 shows that the inorganic matter content was greater in both coal samples compared to olive stones, confirming the results of proximate analysis. The porosity in the coal briquettes was similar regardless of whether resin or starch was used as the binder, indicating that binder type has no influence on coal porosity.

3.3. X-ray diffraction

The XRD analysis of original woodchips and olive stones and torrefied material indicated the formation of crystalline pattern correlated to the cellulose structure, as shown in the supplemental material (Figs. S-29-S-31). The broad reflections at 15, 22.5 and 35° show the development of a crystalline phase, where the c axis of the crystal is parallel to the cellulose chain axis [61]. The XRD reflections of raw biomass and torrefied material were similar, indicating no significant influence of heat treatment temperature and biomass origin on the structure of torrefied woodchips and olive stones. The XRD results showed that torrefied olive stones and anthracite exhibit reflections from crystalline silicon oxides. In addition, olive stones and torrefied olive stones contain a few reflections from crystalline whewellite, whereas anthracite contains sharp and narrow reflections from kaolinite [62,63].

3.4. Thermodynamic calculations with FactSage

Equilibrium calculations were conducted in order to establish the major inorganic components in the woodchips, olive stones, torrefied biomass and anthracite based on the ash composition analysis (Table 1). The elements were assumed to be present in gaseous or condensed phases at thermodynamic equilibrium e.g. chlorine exists as HCl (gas) and KCl (s). The calculations showed that the differences in inorganic composition using either FToxid or GTOX databases are small, as shown in the supplemental material (Fig. S-18-S-27). Thermodynamic calculations both databases showed the presence of sulfur-containing compounds (pyrrhotite

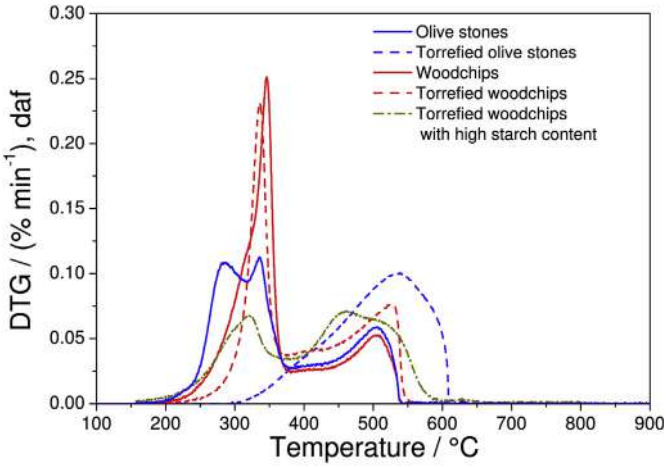

(a): Biomass

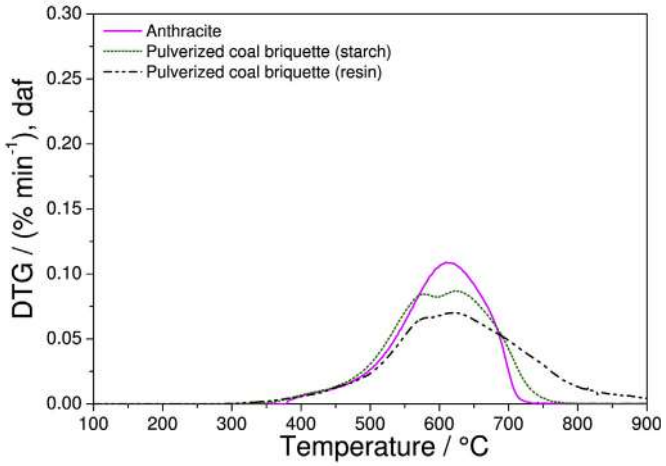

(b): Coal

Fig. 2. DTG curves of raw olive stones and woodchips, torrefied material, torrefied woodchips with high starch content, anthracite, and pulverized coal briquettes using starch or resin as a binder reacted in 20% volume fraction CO_2 + 80% volume fraction N_2.

or iron sulphides), confirming the results of Defoort et al. [64]. The results of calculations using the FToxid database indicated the presence of hydroxy-based compounds in biomass and coal (i.e. $Ca_5HO_{13}P_3$, $KMg_3AlSi_3O_{10}(OH)_2$) [65]. The calculations also showed that potassium chloride (KCl), chrome phlogopite ($KMg_3AlSi_3O_{10}(OH)_2$), calcium carbonate ($CaCO_3$), butschliite ($K_2Ca(CO_3)_2$), devitrite ($Na_2Ca_3Si_6O_{16}$), olivine, and potassium phosphate magnesiumphosphate ($KPMgO_4$) are present in the raw woodchips and olive stones. In addition to the inorganic compounds found in a raw biomass, the torrefied samples contained silicates (wollastonite, clinopyroxene) and silicon oxides (SiO_2) depending on the amount of Si. The major inorganic compound detected in equilibrium calculations of anthracite was silica. Alumina (corundum) was calculated as a minor constituent among other phases (sulfides, feldspar). The discrepancies in calculations can be explained by the possible incompleteness of databases used for such complex systems. As an example, hydroxy-based phases have not been yet included into the oxide database GTOX. Therefore, the data from SGPS is not comparable with GTOX. Sulfur-containing phases in FToxid database were considered separately and thus, they appear as stoichiometric compounds and not as solutions.

3.5. SEM analysis

Fig. 4 illustrates that torrefaction and briquetting have no influence on the morphology of biomass and coal. The outer surface of olive stones and torrefied material exhibits a glassy shell, large cavities and macropores, as shown in Fig. 4(a)-4(b). Torrefied woodchips preserved the structure of an original biomass particle with the longitudinal tracheids and resin vessels, as shown in Fig. 4(c) and supplemental material (Fig. S-7). Particles of woodchips and torrefied material displayed a smooth outer surface and a large number of macropores. The anthracite and pulverized coal briquette particles developed a small fraction of macropores, as shown in Fig. 4(e)-4(f). In addition, particles of pulverized coal briquette had agglomerated. The blue lines marked regions on the coal surface indicated the incorporation of inorganic matter into the anthracite structure.

3.6. Mercury intrusion porosimetry

Table 4 summarizes the characteristics of raw olive stones and woodchips, torrefied material, anthracite, and coal briquettes using starch or resin as a binder with regards to porosity, pore size and specific surface area. Porosity by skeleton density of olive stones and woodchips increased from 20.1 to 49.6% and from 57.4 to 69.4%, indicating that torrefaction has a significant influence. Olive stones developed a greater macroporosity and obtained a greater median pore size during torrefaction, whereas the excesses of the starch addition led to only slight increase in macroporosity. Addition of a binding agent led to pore collapse in the torrefied biomass briquette which increased the macroporosity and decreased the amount of micro and mesopores [66]. The macroporosity of torrefied woodchips remained similar to that of the raw material. Raw woodchips were more macroporous than raw olive stones. Thus, addition of starch had less influence on the macroporosity of woodchip particles than during briquetting of torrefied olive stones. The decreased cumulative pore volume of briquettes from torrefied material was related to the poor accessibility of biomass particles due to blockage of pores by starch. Table 4 shows that briquetting had only a slight influence on porosity of anthracite using starch or resin as a binder. The median pore diameter of anthracite briquettes was less than that of raw feedstock and torrefied material. Similarly, for the torrefied biomass briquette, macroporosity and macropore size of anthracite briquettes increased. Results show that porosity and pore size of coal briquettes using different binder agents remained nearly similar, indicating that selection of a binder has no influence on the properties of coal particles in a briquette.

3.7. Particle size and shape

Fig. 5 shows particle size distributions for anthracite, olive stones, torrefied olive stones and coal sample before briquetting, characterized using sieving, 2D dynamic imaging and laser diffraction. The data obtained by different particle size characterization techniques is repeatable, as shown in the supplemental material (Fig. S-2). The particle size analysis indicated that coal samples before briquetting contained a larger fraction of small particles compared to anthracite due to mechanical crushing. The torrefied olive stone particle size distribution was similar to the raw biomass. 2D dynamic imaging produced very similar size distributions for all biomass samples.

Moreover, sieving and 2D dynamic imaging produced very similar size distributions for coal and biomass samples, while a significant deviation was observed when compared with the results obtained from laser diffraction. Particle shape was characterized

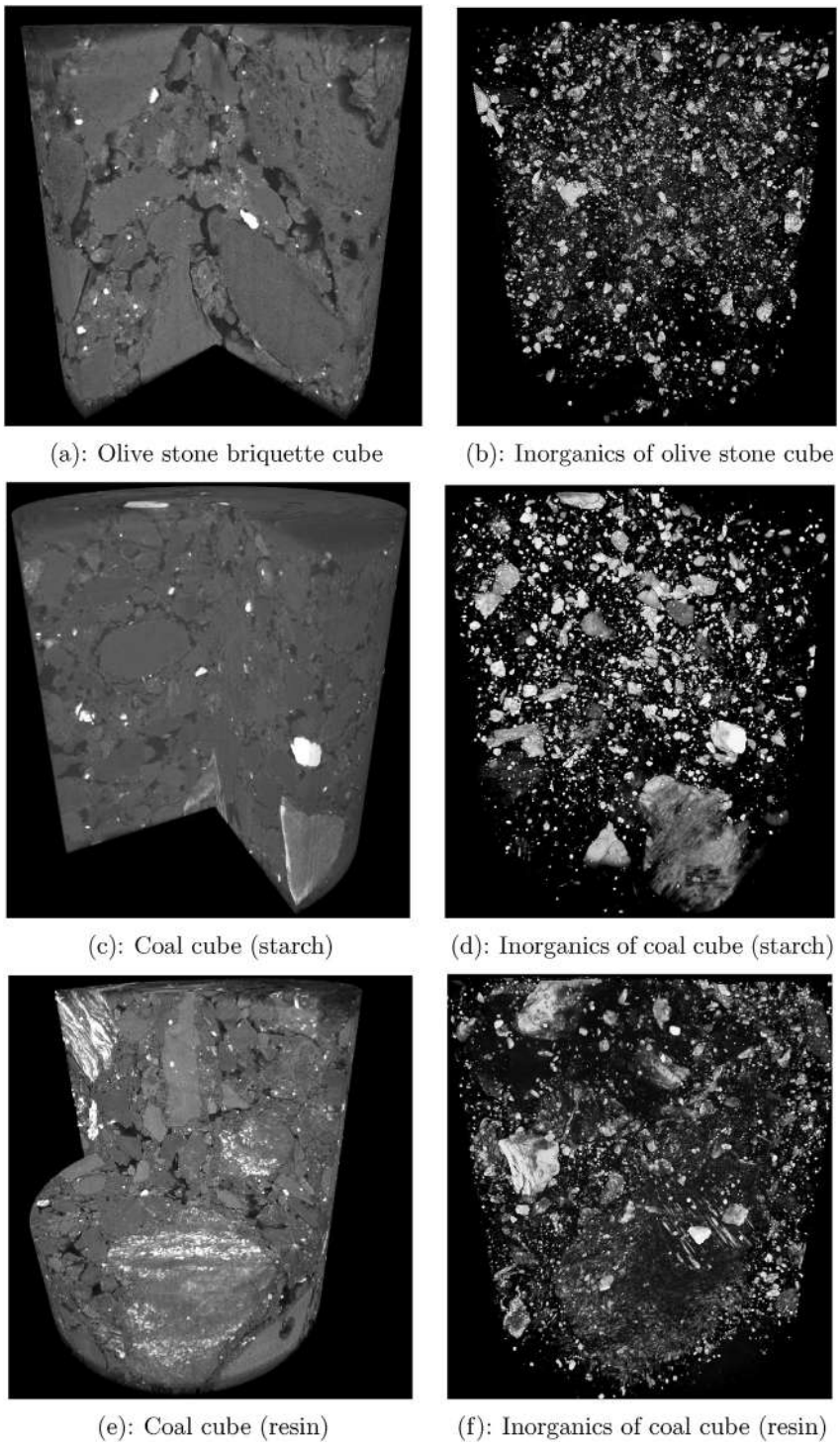

Fig. 3. XμCT imaging analysis of biomass briquette using starch binder and coal briquettes using starch or resin binder. Figures (b,d,f) show the inorganic matter in briquettes with the bright volumetric areas.

Table 3
3D quantitative analysis of olive stone and coal briquettes.

Sample	Phase, %		
	Feedstock	Binder	Inorganic matter
Olive stone briquette	80.5	19	0.5
Coal briquette (starch)	91.6	7	1.5
Coal briquette (resin)	84.7	13.3	2

using 2D dynamic imaging instrument. Small anthracite particles of size <0.5 mm were slightly more elongated and less spherical (SPHT = 0.78 and aspect ratio AR = 0.72) than large particles (SPHT = 0.82 and aspect ratio AR = 0.76). The difference in sphericity and aspect ratio AR was caused by strong particle edge deformation of small anthracite particles during comminution, as shown in the supplemental material (Fig. S-3). The aspect ratio of torrefied olive stones particles measured by 2D dynamic imaging

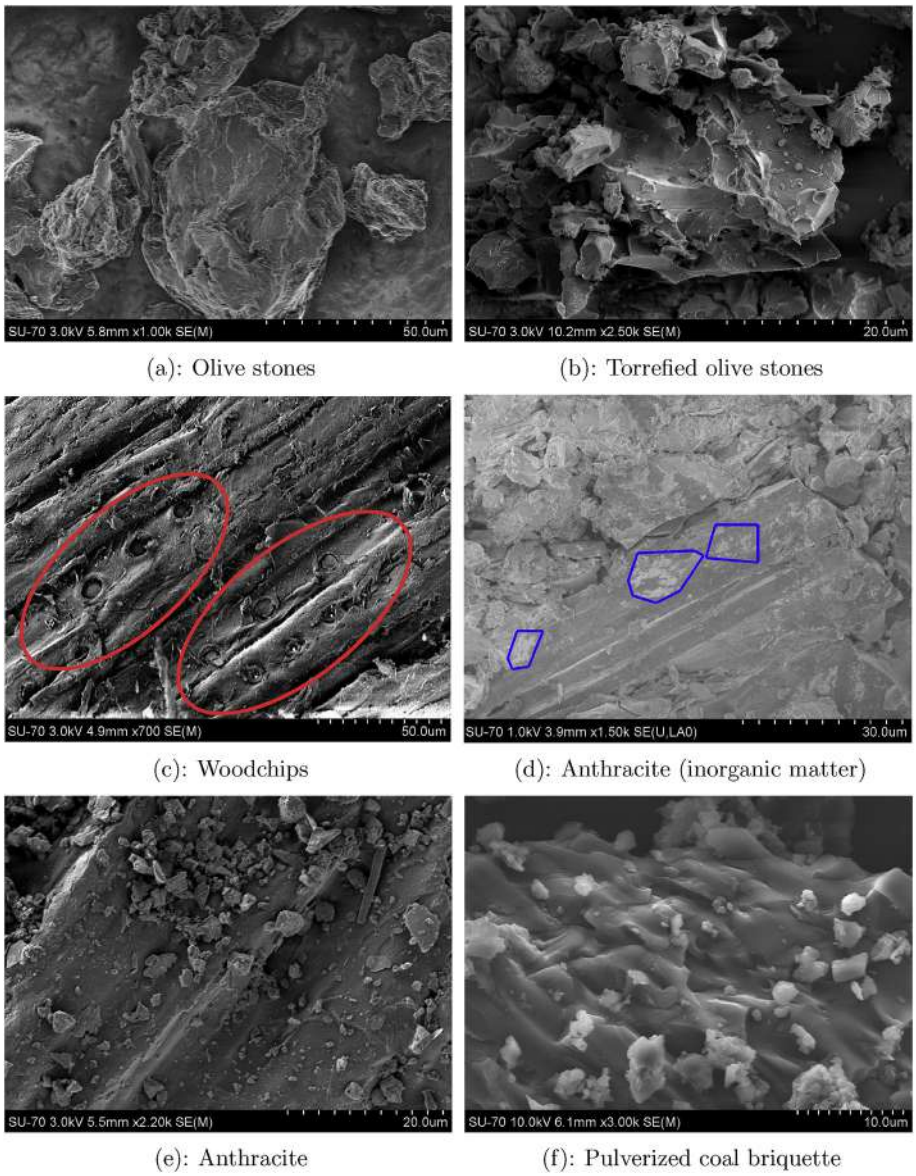

Fig. 4. SEM analysis of olive stones, torrefied olive stones, woodchips, anthracite and pulverized coal briquette using starch as a binder. The macropores on woodchips particles are marked with red ovals. The blue lines show the inorganic matter on the coal surface. Results of ash elemental analysis using the SEM-EDS technique will be correlated to the coal morphology below. (For interpretation of the references to colour in this figure legend, the reader is referred to the Web version of this article.)

over $x_{Ma\,min}$ remained similar to the raw biomass. The sphericity of coal (mean SPHT of all samples = 0.62) and the aspect ratio (mean AR of all samples = 0.64) indicate that the olive stones and coal were nearly square-shaped [67]. Overall, 2D dynamic imaging analysis showed that the particles of a different size had square shapes and that the ratio between particle dimensions did not change significantly with decreasing particle size, which is in line with the results of Cardoso et al. [68].

3.8. Solid-state NMR spectroscopy

The effect of feedstock origin on the organic matter transformation in torrefaction and briquetting process was monitored using ^{13}C CP/MAS spectroscopy, as shown in Fig. 6. The assignment of resonances is shown in the supplemental material (Table S-4). Based on the ^{13}C CP/MAS spectra, both the original woodchips and olive stones showed similar compositions, typical for polysaccharides with abundant compounds. Compositional differences were mainly observed for the carbohydrates in the original olive stones.

The composition of woodchips changed only slightly as a result of torrefaction and with addition of larger fraction of starch binder to the torrefied material. The major compositional difference in the woodchip structure was related to the appearance of a distinct peak at 31 ppm originating from methylene resonance. The spectra of torrefied olive stones are characterized by a broad resonance centered at 157.5, 150.2, and 128 ppm originating from aromatics [69,70]. These spectral peaks indicate the aromatization of olive stones during the torrefaction process and the formation of turbostratic structures [71]. Differences in composition between the torrefied woodchips and olive stone were related to the slightly higher heat treatment temperature during torrefaction of olive stones. The spectra of anthracite and coal briquette with intense resonances centered at 125.1, 34.7, and 20.2 ppm correspond to hydrogenated polyaromatic carbons and aliphatic peaks with the attached methylene and methyl groups [72,73]. No changes in the

Table 4
Porosity and pore size of raw biomass and coal, torrefied material with low or high binder contents and briquettes using starch or resin as binding agents, characterized by mercury intrusion porosimeter and helium pycnometer.

Parameter	Olive stones	Torrefied olive stones	Woodchips	Torrefied woodchips	Torrefied woodchips high starch content
Skeletal density, g cm^{-3}	1.5	1.7	1.5	1.5	1.5
Porosity by Hg intrusion, %	20.1	49.6	57.4	69.4	41.3
Inaccessible porosity, %	5.8	14.5	8.6	1	16.4
Macropores, %	67.3	84.7	95.2	94.9	96.3
Mesopores, %	11.5	7.2	3.6	3.5	2.4
Micropores, %	21.2	8.1	1.2	1.6	1.3
V_{cum}, mm^3 g^{-1}	1813	796	1119	564	665
SSA, m^2 g^{-1}	18.6	33.1	8.1	9	19
Average pore diameter, μm	0.04	0.1	0.6	0.7	0.1
Median pore diameter, μm	5.3	6.4	7.8	9.4	6.5
Parameter	Anthracite	Coal briquette (starch)	Coal briquette (resin)		
Skeletal density, g cm^{-3}	1.5	1.7	1.4		
Porosity by Hg intrusion, %	49.7	51.6	50.5		
Inaccessible porosity, %	8.7	5.1	4.9		
Macropores, %	88.4	97	96		
Mesopores, %	6.6	1.5	2.5		
Micropores, %	5	1.5	1.5		
V_{cum}, mm^3 g^{-1}	815	635	641		
SSA, m^2 g^{-1}	19.3	10.6	10.4		
Average pore diameter, μm	0.2	0.1	0.1		
Median pore diameter, μm	3	4.5	4.1		

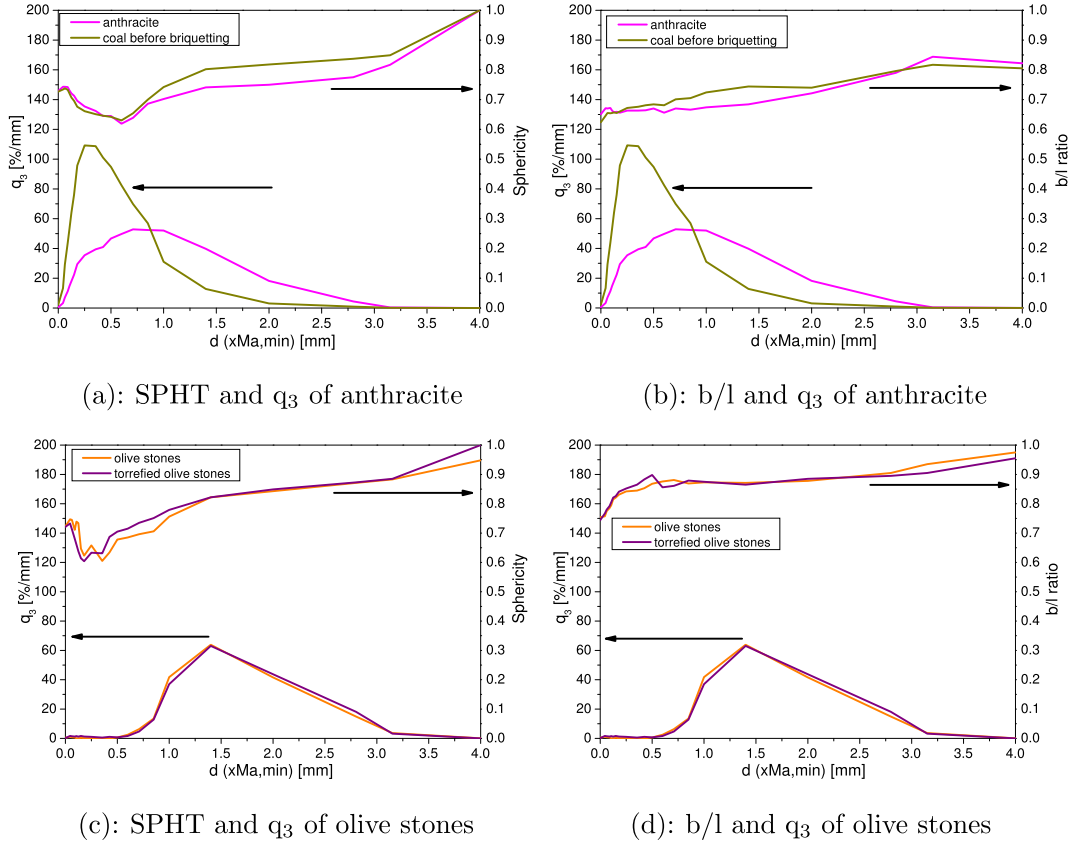

Fig. 5. Particle frequency distribution (q_3), sphericity (SPHT) and width/length ratio (b/l) of: (a–b) anthracite and coal before briquetting; (c–d) raw olive stones and torrefied olive stones before briquetting.

anthracite structure were observed from briquetting.

4. Discussion

The results of this work demonstrated that the use of low quality biomass has the potential to produce high-quality briquettes for the energy sector. The thermogravimetric experiments showed that biomass composition, type and concentration of a binder have a small influence on the properties of briquettes. However, differences in composition of biomass and coal exerted a great influence on the intrinsic reactivity and calorific value of briquette. The reactivity of the briquettes can be affected by differences in ash

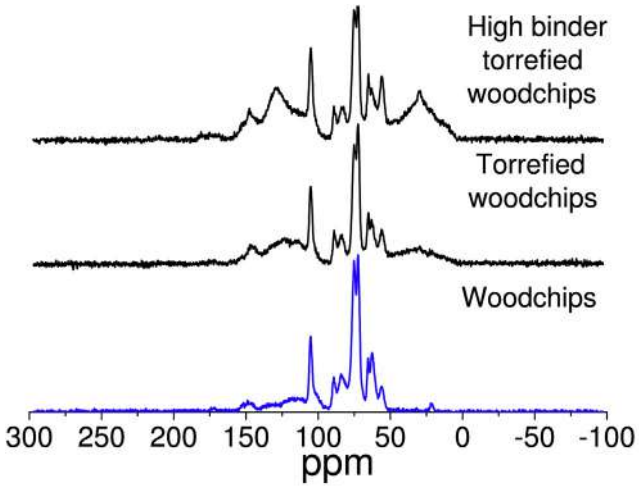

(a): Original and torrefied woodchips

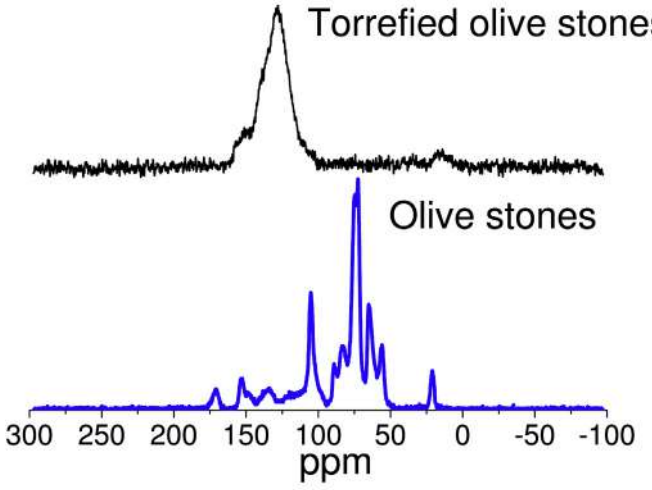

(b): Original and torrefied olive stones

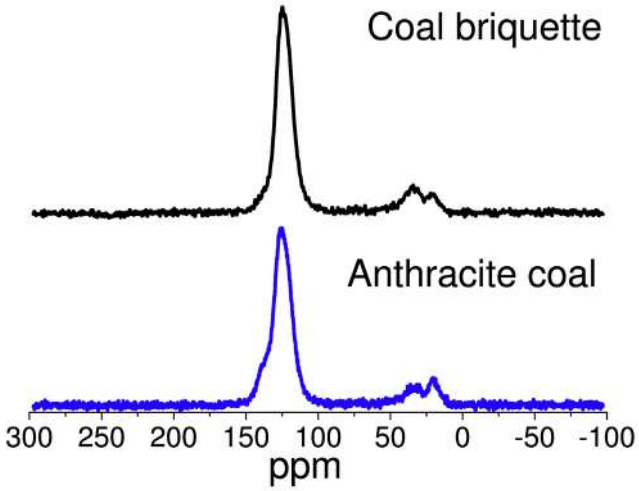

(c): Anthracite and coal briquettes

Fig. 6. Solid-state ^{13}C CP/TOSS MAS NMR spectra of anthracite coal, coal briquettes, original olive stones, torrefied olive stones, original woodchips, torrefied woodchips, and torrefied woodchips with an increased quantity of starch binder. Data was collected at $B_0 = 9.4$ T under MAS at 12 kHz.

composition, carbon chemistry, particle size and porosity of the feedstock [74]. The ash content of native olive stones (0.8 wt. %) was 12 times less than that of anthracite (9.9 wt. %). High amounts of alkali metals in the anthracite samples promote faster devolatilization rates and suppress tar formation, leading to higher char yields and higher CO_2/O_2 reactivity than low ash-containing feedstocks [75]. Thus, based on ash content alone it might be expected that anthracite should be more reactive than the olive stones. However, the anthracite and pulverized coal briquette samples were less reactive than olive stones and torrefied olive stones. The proximate and ultimate analysis showed that anthracite coal is less volatile with a greater carbon content and thus, less reactive than olive stones. The results contained in the supplemental material (Fig. S-28) indicate that the oxygen and hydrogen content in torrefied biomass samples decreases with the higher heat treatment temperature, corresponding to results of Anukam et al. [16]. However, the CO_2 gasification reactivity of torrefied biomass decreased only slightly compared to that of raw feedstock. In addition, the 3D imaging analysis using XμCT technique and mercury intrusion porosimetry both showed that coal particles in a briquette were less porous and smaller in size than olive stones particles, leading to the lower reactivity of milled briquettes compared to other samples. The porosity in anthracite and milled coal briquettes using starch or resin as a binder was similar, whereas the reaction rate of anthracite was 180 times greater than that of milled briquettes. The particle size of milled coal briquette (0.25 mm) was less than that of anthracite (0.95 mm), emphasizing a strong influence of particle size on differences in coal reactivity. The particle size of raw olive stones and torrefied biomass (1.75 mm) was similar, whereas the reaction rate of the raw olive stones was 13 times greater than that of torrefied material, as shown in the supplemental material (Table S-1). This indicates that the particle size plays a less important role in gasification reactivity of torrefied olive stones than the porosity. The reactivities of natural woodchips and olive stones were similar despite the fact that woodchips have a greater content of holocelluloses than olive stones, confirming the previous results of Surup et al. [76]. Moreover, torrefied olive stones were less reactive than torrefied woodchips. The ^{13}C CP/MAS spectra of torrefied material showed that the composition of torrefied olive stones was more aromatic than that of torrefied woodchips due to the slightly higher heat treatment temperature during torrefaction of olive stones.

An innovative approach was developed to characterize the briquette porosity and particle size using XμCT technique. The results showed that the particle size determined using the 2D dynamic imaging analysis was smaller than the particle size determined from XμCT data analysis. In the 2D dynamic imaging, a particle is represented as an ellipsoid with the thickness assumed to be equal to the width. Moreover, the shape of irregular biomass particles is commonly quantified using equivalent shape models (i.e. a sphere, an ellipsoid, a cuboid), leading to the underestimation of the real particle surface area [77]. The XμCT provides three-dimensional visualizations of features in the interior of a specimen from relatively few particles, leading to non-representative particle size analysis [78]. In addition, when a large size range of particles is present, the smaller particles, which cannot be adequately resolved, appear as blurred particles that complicate image processing [79]. In the present work, the anthracite and olive stones particles underwent compression during briquetting, leading to the formation of large particles in the images from XμCT analysis. Three-dimensional image analysis using the XμCT enables the characterization of true physical size of irregular feedstock particles based on the results of Hamdi et al. [80]. The XμCT analysis showed the formation of three solid phases which were related to feedstock carbon content, binder and ash fractions. Previous

studies on XμCT analysis of wheat straw and poplar char pellets showed that the micro-tomography can separate the carbon fraction or inorganic matter that is rich in potassium-calcium silicates and carbon oxides [81]. The literature suggests that the inorganic elements in raw olive stones and torrefied material probably appeared as sylvite (KCl), quartz (SiO_2), calcite ($CaCO_3$), halite (NaCl), arcanite (K_2SO_4), potassium carbonate (K_2CO_3), vuagnatite ($CaAlSiO_4(OH)$) and dolomite ($CaMg(CO_3)_2$), as reported by Romero et al. [82]. Moreover, calcite and quartz in raw olive stones could be present in a greater concentration than other compounds [83]. The elements in the coal briquette probably formed kaolinite ($Al_2Si_2O_5(OH)_4$), quartz (SiO_2), mullite ($3Al_2O_32SiO_2$), and calcite ($CaCO_3$) [84–86]. In the present work, SEM-EDS and ash elemental analysis using ICP showed that the inorganic matter composition of raw olive stones and torrefied material was similar due to the relatively low heat treatment temperature [15,87,88]. The SEM-EDS analysis showed that the main elements forming the inorganic phase of torrefied olive stones and pulverized coal briquette were Si, Na, Al, K, Ca, Mg, Cl, and S, as shown in the supplemental material (Fig. S-17). The comparison of thermodynamic equilibrium calculation and X-ray diffraction results indicated that calcium, potassium, silicon and alumina-containing compounds were dominant in torrefied olive stones and pulverized coal briquette. The X-ray diffraction results clearly suggested that the bright volumetric areas in all scanned materials were rich in quartz. Moreover, no large differences were observed in reconstructed microtomography images among pulverized coal briquettes using starch or resin as a binder. This indicates that the addition of a binder has no impact on the ash composition of coal briquettes.

The addition of natural binders in briquettes comprised of torrefied biomass or coal is important to make durable particle-particle bonding [22]. The calorific value of briquettes from anthracite and torrefied biomass increased only slightly with an increase in the amount of binder added. Higher treatment temperatures led to increased carbonization of olive stones with no further impact on the calorific value of briquettes, confirming the previous results of Benavente and Fullana [3]. However, the ^{13}C CP/MAS spectra indicated that the organic structure of biomass and coal is different. Anthracite contains a great amount of hydrogenated polycyclic aromatic rings arranged in a linear catenation order, whereas biomass samples are rich in polysaccharides, proteins, lipids and other abundant compounds [89,90]. The high moisture content in original woodchips and olive stones could also have a strong impact on the calorific value of torrefied biomass briquette, confirming the previous results of Demirbas [91]. The moisture content, calorific value and bulk density of non-treated biomass depend upon the feedstock origin [92]. A reduced moisture and volatile matter content of biomass can improve the calorific value with the increased torrefaction temperature [93]. The results of the present work clearly show that the differences in organic composition and moisture content of biomass and coal have the most significant influence on the calorific value of briquettes.

5. Conclusion

Low quality feedstocks were converted into high-quality briquettes by torrefaction treatment and their properties were compared with the coal briquettes. The resulting materials were studied for reactivity, composition and structure. Thermogravimetric analysis results showed that the CO_2 reactivities of torrefied material and coal depend mainly on heat treatment temperature, organic composition of feedstock and porosity of material, and less on the ash composition of the original feedstocks. Differences in calorific value were ascribed in part to differences in moisture content and feedstock organic composition, as evaluated by ^{13}C CP/MAS and proximate analysis. An innovative approach was developed to characterize the feedstock porosity using XμCT technique that identified three solid phases in a briquette. The inorganic fraction in torrefied biomass and coal briquettes contained quartz retaining in particles from natural feedstock. Torrefaction of low quality biomass showed a great promise for producing torrefied biomass briquettes with reactivity comparable to coal briquettes. The findings of this study emphasize the potential use of torrefied low quality biomass in the energy sector, with concomitant reduction in CO_2 emissions.

Acknowledgements

The authors gratefully acknowledge financial support from the Science Foundation Ireland (Grant number 16/SP/3829) and Arigna Fuels under the Sustainable Energy and Fuel Efficiency (SEFE) spoke of the Research Centre for Marine and Renewable Energy (MaREI). Michael Byrne, Dr. Sergey Beloshapkin from University of Limerick, Gerrit Ralf Surup from University of Agder, Gundula Stein from GNF Berlin, and Dr. Denis Ring from the University College Cork are acknowledged for the technical support on XμCT, SEM-EDS, laser diffraction analysis, mercury intrusion porosimetry, helium pycnometry, and CAMSIZER measurements.

Appendix A. Supplementary data

Supplementary data to this article can be found online at https://doi.org/10.1016/j.energy.2019.01.064.

References

[1] Bullock C, Hawe J, Little D. Realising the ecosystem-service value of native woodland in Ireland. N Z J For Sci 2014;44:1–10.
[2] Pawelczyk A. EU policy and legislation on recycling of organic wastes to agriculture. ISAH 2005;1:64–71.
[3] Benavente V, Fullana A. Torrefaction of olive mill waste. Biomass Bioenergy 2015;73:186–94.
[4] Rodriguez G, Lama A, Rodriguez R, Jimenez A, Guillen R, Fernandez-Bolanos J. Olive stone an attractive source of bioactive and valuable compounds. Bioresour Technol 2008;99:5261–9.
[5] Sanchez F, San Miguel G. Improved fuel properties of whole table olive stones via pyrolytic processing. Biomass Bioenergy 2016;92:1–11.
[6] Ren X, Sun R, Meng X, Vorobiev N, Schiemann M, Levendis YA. Carbon, sulfur and nitrogen oxide emissions from combustion of pulverized raw and torrefied biomass. Fuel 2017;188:310–23.
[7] Jansson S. Thermal formation and chlorination of dioxins and dioxin-like compounds. PhD thesis. Umeå University; 2008.
[8] Mitchell EJS, Lea-Langton AR, Jones JM, Williams A, Layden P, Johnson R. The impact of fuel properties on the emissions from the combustion of biomass and other solid fuels in a fixed bed domestic stove. Fuel Process Technol 2016;142:115–23.
[9] Medic C, Darr M, Shah A, Potter B, Zimmermann J. Effects of torrefaction process parameters on biomass feedstock upgrading. Fuel 2012;91(1):147–54.
[10] Hamid MF, Idroas MY, Ishak MZ, Zainal Alauddin ZA, Miskam MA, Abdullah MK. An experimental study of briquetting process of torrefied rubber seed kernel and palm oil shell. BioMed Res Int 2016;1:1–11.
[11] Thrän D, Witt J, Schaubach K, Kiel J, Carbo M, Maier J, et al. Moving torrefaction towards market introduction - technical improvements and economic-environmental assessment along the overall torrefaction supply chain through the SECTOR project. Biomass Bioenergy 2016;89:184–200.
[12] Araujo S, Almeida Vilas Boas M, Neiva DM, Vital B, de Cassia Carneiro A, Breguez M, et al. Effect of a mild torrefaction for production of eucalypt wood briquettes under different compression pressures. Biomass Bioenergy 2016;90:181–6.
[13] Felfli FF, Luengo CA, Suarez JA, Beaton PA. Wood briquette torrefaction. Energy Sust Develop 2005;9(3):19–22.
[14] Tumuluru JS, Kuang X, Sokhansanj S, Lim CJ, Bi X, Melin S. Development of laboratory studies on the off-gassing of wood pellets. Can Biosyst Eng 2010;52(8):8.1–9.
[15] Shoulaifar TK, DeMartini N, Zevenhoven M, Verhoeff F, Kiel J, Hupa M. Ash-forming matter in torrefied birch wood: changes in chemical association. Energy Fuels 2013;27:5684–90.
[16] Anukam A, Mamphweli S, Reddy P, Okoh O, Meyer E. An investigation into the impact of reaction temperature on various parameters during torrefaction of

sugarcane bagasse relevant to gasification. J Chem 2015;235163:1–12.
[17] Strandberg M, Olofsson I, Pommer L, Wiklund-Lindström S, Åberg K, Nordin A. Effects of temperature and residence time on continuous torrefaction of spruce wood. Fuel Process Technol 2015;134:387–98.
[18] Shang L, Ahrenfeldt J, Holm JK, Sanadi AR, Talbro Barsberg S, Thomsen T, et al. Changes of chemical and mechanical behavior of torrefied wheat straw. Biomass Bioenergy 2012;40:63–70.
[19] Cellatoglu N, Ilkan M. Torrefaction of solid olive mill residue. Bioresources 2015;10(3):5876–89.
[20] Peng JH, Bi HT, Lim CJ, Sokhansanj S. Study on density, hardness, and moisture uptake of torrefied wood pellets. Energy Fuels 2013a;27:967–74.
[21] Peng JH, Bi HT, Sokhansanj S, Lim CJ. Torrefaction and densification of different species of softwood residues. Fuel 2013b;111:411–21.
[22] Kaliyan N, Morey RV. Strategies to improve durability of switchgrass briquettes. Trans ASABE (Am Soc Agric Biol Eng) 2009;52(6):1943–53.
[23] Tabil LG. Binding and pelleting characteristics of alfalfa. PhD thesis. University of Saskatchewan; 1996.
[24] Thomas M, van Zuilichem DJ, van der Poel AFB. Physical quality of pelleted animal feed. 2. Contribution of processes and its conditions. Anim Feed Sci 1997;64(2–4):173–92.
[25] Taulbee D, Patil DP, Honaker RQ, Parekh BK. Briquetting of coal fines and sawdust. Part I: binder and briquetting parameters evaluations. Int J Coal Prepar Util 2009;29:1–22.
[26] Okafor IF, Anyanwu CN. Production of smokeless briquette fuel from subbituminous coal for domestic and industrial uses. Sci J Energy Eng 2015;3(4):33–9.
[27] Burchill P, Hallam GD, Lowe AJ, Moon N. Studies of coals and binder systems for smokeless fuel briquettes. Fuel Process Technol 1994;41:63–77.
[28] Cobb JT, Akers DJ. Co-processed fuel pellets from coal, biomass, and waste. Div Fuel Chem 2001;46:715–6.
[29] Kural OO, Savasci T, Eskikaya S, APP. A new binder for briquetting lignites. Fuel 1989;68(3):404–7.
[30] Yaman S, Sahan M, Haykiri-Acma H, Sesen S, Kücükbayrak S. Fuel briquettes from biomass-lignite blends. Fuel Process Technol 2001;72(1):1–8.
[31] Nwakaire JN, Ugwuishiwu BO. Development of a Natural Cross Draft Gasifier Stove for Application in Rural Communities in Sub-Saharan Africa. J Appl Sci 2015;15(9):1149–57.
[32] Deng J, Wang GJ, Kuang JH, Zhang YL, Luo YH. Pretreatment of agricultural residues for co-gasification via torrefaction. J Anal Appl Pyrolysis 2009;86:331–7.
[33] Trubetskaya A, Hofmann Larsen F, Shchukarev A, Ståhl K, Umeki K. Potassium and soot interaction in fast biomass pyrolysis at high temperatures. Fuel 2018;225(1):89–94.
[34] Coats AW, Redfern JP. Kinetic parameters from thermogravimetric data. Nature 1964;201:68–9.
[35] Joffre T, Girlanda O, Forsberg F, Sahlén F, Sjödahl M, Gamstedt EK. A 3D in-situ investigation of the deformation in compressive loading in the thickness direction of cellulose fiber mats. Cellulose 2015;22:2993–3001.
[36] Forsberg F, Mooser R, Arnold M, Hack E, Wyss P. 3D micro-scale deformations of wood in bending: synchrotron radiation μCT data analyzed with digital volume correlation. J Struct Biol 2008;164:255–62.
[37] Forsberg F, Sjödahl M, Mooser R, Hack E, Wyss P. Full three-dimensional strain measurements on wood exposed to three-point bending: analysis by use of digital volume correlation applied to synchrotron radiation micro-computed tomography image data. Strain 2010;46:47–60.
[38] Gamble JF, Terada M, Holzner C, Lavery L, Nicholson SJ, Timmens P, et al. Application of X-ray microtomography for the characterisation of hollow polymer-stabilised spray dried amorphous dispersion particles. Int J Pharm 2016;510:1–8.
[39] Otsu N. A threshold selection method from gray-level histograms. IEEE Transactions on systems, man, and cybernetics 1979;9(1):62–6.
[40] Bale CW, Belisle E, Chartrand P, Decterov SA, Eriksson G, Gheribi AE. FactSage thermochemical software and databases, 2010-2016. Calphad 2016;54:35–53.
[41] Hack K, Jantzen T, Müller M, Yazhenskikh E, Wu G. A novel thermodynamic database for slag systems and refractory materials. In: Proceedings 5th Int Congress Sci Tech Steelmaking, ICS Dresden; 2012. p. 1–15.
[42] Plötze M, Niemz P. Porosity and pore size distribution of different wood types as determined by mercury intrusion porosimetry. Europ J Wood Wood Product 2011;69(4):649–57.
[43] Yin J, Song K, Lu Y, Zhao G, Yin Y. Comparison of changes in micropores and mesopores in the wood cell walls of sapwood and heartwood. Wood Sci Technol 2015;49:987–1001.
[44] Washburn EW. Note on a method of determining the distribution of pore sizes in a porous material. Proc Natl Acad Sci Unit States Am 1921;7:115–6.
[45] Junghaus K, Niemz P, Bächle F. Untersuchungen zum Einfluss der thermischen Vergütung auf die Porosität von Fichtenholz. Holz Roh Werkst 2005;63(3):243–4.
[46] ISO 15901-1. Evaluation of pore size distribution and porosity of solid materials by mercury porosimetry and gas adsorption - Part 1: mercury porosimetry. Geneva: International Organization for Standardization; 2016.
[47] DIN 66137-2, Determination of solid state density - Part 2: Gaspycnometry. Germany: Deutsches Institut Für Normung E.V.
[48] Morcombe CR, Zilm KW. Chemical shift referencing in MAS solid state NMR. Magnes Res 2003;162:479–86.
[49] Antzutkin ON. Sideband manipulation in magic-angle-spinning nuclear magnetic resonance. Prog Nucl Magn Reson Spectrosc 1999;35:203–66.
[50] Song Z, Antzutkin ON, Feng Z, Levitt MH. Sideband suppression in magic-angle-spinning NMR by a sequence of 5 π pulses. Solid State Nucl Magn Reson 1993;2:143–6.
[51] Fung B, Khitrin AK, Ermolaev K. An improved broadband decoupling sequence for liquid crystals and solids. J Magn Reson 2000;142:97–101.
[52] Sluiter A, Hames B, Ruiz R, Scarlata C, Sluiter J, Templeton D, et al. Determination of structural carbohydrates and lignin in biomass. Golden (CO): National Renewable Energy Laboratory; 2011 July. Report No. NREL/TP-510-42618. Contract No.: DE-AC36-08-GO28308.
[53] Willför S, Hemming J, Leppänen AS. Analysis of extractives in different pulps - method development, evaluation, and recommendations. Finland: Åbo Akademi University, Laboratory of Wood and Paper Chemistry; 2004-2009. Report No. B1 of the EU COST E41 action "Analytical tools with applications for wood and pulping chemistry.
[54] Hames B, Ruiz R, Scarlata C, Sluiter J, Sluiter A. Preparation of samples for compositional analysis. Golden (CO): National Renewable Energy Laboratory; 2011. June Report No. NREL/TP-510-42620. Contract No.: DE-AC36-99-GO10337.
[55] Thammasouk K, Tandjo D, Penner MH. Influence of extractives on the analysis of herbaceous biomass. J Agric Food Chem 1997;45:437–43.
[56] Caballero JA, Conesa JA, Font R, Marcilla A. Pyrolysis kinetics of almond shells and olive stones considering their organic fractions. J Anal Appl Pyrolysis 1997;42:159–75.
[57] Gomez-Martin A, Chacartegui R, Raminez-Rico J, Martinez-Fernandez J. Performance improvement in olive stone's combustion from a previous carbonization transformation. Fuel 2018;228:254–62.
[58] Xue G, Kwapinska M, Kwapinska W, Czajka KM, Kennedy J, Leahy JJ. Impact of torrefaction on properties of *Miscanthus x giganteus* relevant to gasification. Fuel 2014;121:189–97.
[59] Zolin A. Reactivity of solid fuels. PhD thesis. Technical University of Denmark; 2001.
[60] Meszaros E, Jakab E, Varhegyi G, Bourke J, Manley-Harris M, Nunoura T, et al. Do all carbonized charcoals have the same chemical structure? 1. Implications of thermogravimetry - mass spectrometry measurements. Ind Eng Chem Res 2007;46(18):5943–53.
[61] French AD. Idealized powder diffraction patterns for cellulose polymorphs. Cellulose 2014;21(2):885–96.
[62] Suarez-Garcia F, Martinez-Alonso A, Fernandez Llorente M, Tascon JMD. Inorganic matter characterization in vegetable biomass feedstocks. Fuel 2002;81:1161–9.
[63] Ward CR, Christie PJ. Clays and other minerals in coal seams of the Moura-Baralaba area, Bowen Basin, Australia. Int J Coal Geol 1994;25:287–309.
[64] Defoort F, Dupont C, Durruty J, Guillaudeau J, Bedel L, Ravel S, et al. Thermodynamic study of the alkali release behavior during steam gasification of several biomasses. Energy Fuels 2015;29:7242–53.
[65] Decterov SA. Thermodynamic database for multicomponent oxide systems. Chimica Techno Acta 2018;5(1):16–48.
[66] Li S, Wang CA, Zhou J. Effect of starch addition on microstructure and properties of highly porous alumina ceramics. Ceram Int 2013;39:8833–9.
[67] Trubetskaya A, Beckmann G, Wadenbäck J, Holm JK, Velaga SP, Weber R. One way of representing the size and shape of biomass particles in combustion modeling. Fuel 2017;206:675–83.
[68] Cardoso CR, Oliveira TJP, Santana Junior JA, Ataide CH. Physical characterization of sweet sorghum bagasse, tobacco residue, soy hull and fiber sorghum bagasse particles: density, particle size and shape distributions. Powder Technol 2013;245:105–14.
[69] Bardet M, Gerbaud G, Giffard M, Doan C, Hediger S, Pape LL. ^{13}C high-resolution solid-state NMR for structural elucidation of archaeological woods. Prog Nucl Magn Reson Spectrosc 2009;55(3):199–214.
[70] Bardet M, Maron S, Foray MF, Berger M, Guillermo A. Investigation of γ-irradiated vegetable seeds with high-resolution solid-state ^{13}C NMR. Radiat Res 2004;161(4):458–63.
[71] Freitas JCC, Emmerich FG, Bonagamba TJ. High-resolution solid-state NMR study of the occurrence and thermal transformations of silicon-containing species in biomass materials. Chem Mater 2000;12(3):711–8.
[72] Premovic PI, Nikolic RS, Premovic MP. Comparison of Solid State ^{13}C NMR of algal coals/anthracite and charcoal-like fusinites: further evidence for graphitic domains. Eur Coal Geol Tech 1997;125:201–5.
[73] Diaz C, Blanco CG. NMR: a powerful tool in the characterization of coal tar pitch. Energy Fuels 2003;17:907–13.
[74] Di Blasi C. Combustion and gasification rates of lignocellulosic chars. Prog Energy Combust Sci 2009;35:121–40.
[75] Niksa S. Predicting the rapid devolatilization of diverse forms of biomass with bio-Flashchain. Proc Combust Inst 2000;28(2):2727–33.
[76] Surup GR, Heidelmann M, Kofoed Nielsen H, Trubetskaya A. Characterization and reactivity of charcoal from high temperature pyrolysis (800-1600°C). Fuel 2019;235(1):1544–54.
[77] Erdogan ST. Simple estimation of the surface area of irregular 3D particles. J Mater Civ Eng 2016;28(8):1–10.
[78] Luerkens DW. Theory and application of morphological and analysis: fine particles and surfaces. CRC Press; 1991.
[79] Erdogan ST, Garboczi EJ, Fowler DW. Shape and size of microfine aggregates: X-ray microcomputed tomography vs. laser diffraction. Powder Technol

2007;177:53–63.
[80] Hamdi SE, Delisee C, Malvestio J, Da Silva N, Le Duc A, Beaugrand J. X-ray computed microtomography and 2D image analysis for morphological characterization of short lignocellulosic fibers raw materials: a benchmark survey. Composites Part A 2015;76:1–9.
[81] Strandberg A, Thyrel M, Skoglund N, Lestander TA, Broström M, Backman R. Biomass pellet combustion: cavities and ash formation characterized by synchrotron X-ray micro-tomography. Fuel Process Technol 2018;176:211–20.
[82] Romero E, Quirantes M, Nogales R. Characterization of biomass ashes produced at different temperatures from olive-oil-industry and greenhouse vegetable wastes. Fuel 2017;208:1–9.
[83] Elouear Z, Bouzid J, Boujelben N, Feki M, Montiel A. The use of exhausted olive cake ash (EOCA) as a low cost adsorbent for the removal of toxic metal ions from aqueous solutions. Fuel 2008;87:2582–9.
[84] Raask E. Mineral impurities in coal combustion: behavior, problems, and remedial measures. Springer; 1985.
[85] Palmer CA, Lyons PC. Selected elements in major minerals from bituminous coal as determined by INAA: implications for removing environmentally sensitive elements from coal. Int J Coal Geol 1996;32:151–66.
[86] Manoj B. A comprehensive analysis of various structural parameters of Indian coals with the aid of advanced analytical tools. Int J Coal Sci Technol 2016;3(2):123–32.
[87] Olsson JG, Jäglid U, Pettersson JBC. Alkali metal emission during pyrolysis of biomass. Energy Fuels 1997;11:779–84.
[88] Blasi CD, Branca C, D'Errico G. Degradation characteristics of straw and washed straw. Thermochim Acta 2000;364:133–42.
[89] Yang F, Hou Y, Wu W, Liu Z. Structures of aromatic clusters of different coals based on benzene carboxylic acids from coal via oxidation. Energy Fuels 2017;31(11):12072–80.
[90] Liu S, Zhu Y, Wu F, Meng W, Wang H, Guo W, et al. Using solid ^{13}C NMR coupled with solution ^{31}P NMR spectroscopy to investigate molecular species and lability of organic carbon and phosphorus from aquatic plants in Tai Lake, China. Environ Sci Pollut Res 2017;24:1880–9.
[91] Demirbas A. Effects of moisture and hydrogen content on the heating value of fuels. Energy Sources, Part A Recovery, Util Environ Eff 2007;29(7):649–55.
[92] Saeed MA, Ahmad SW, Kazmi M, Mohsin M, Feroze N. Combined effects of torrefaction and pelletization parameters on the quality of pellets produced from torrefied biomass. Pol J Chem Technol 2015;17(2):23–8.
[93] Rudolfsson M, Boren E, Pommer L, Nordin A, Lestander TA. Combined effects of torrefaction and pelletization parameters on the quality of pellets produced from torrefied biomass. Appl Energy 2017;191:414–24.